The Mesogranulation Convective Power Spectrum

Laurence J. November

La Luz Physics, La Luz NM 88337-0217 USA
laluzphys@yahoo.com
July 3, 2018

Abstract

Some authors have pointed out that the observed spectrum of long-lived solar horizontal velocity shows only a single peak at wavelength ≃35 Mm, 'supergranulation'. However the corresponding vertical-velocity spectrum looks very different with power shifted to higher wavenumber in a broad divided peak representing a range of plume sizes or half wavelengths from 4–12 Mm, i.e. 'mesogranulation'. Vertical-velocity spectra derived from the Hathaway *et al.* (2000) SOHO-MDI 62 day full-disk Doppler-velocity spectrum and based upon the Koutchmy (1994) granulation intensity spectrum show expected Kolmogorov-inertial and eddy-noise power-law wavenumber subranges, giving evidence for energy injection into the vertical flow around three coherent length scales ≳1.01, 5.4, and 10.5 Mm, i.e. granulation, and 'mesogranular' and 'supergranular' *subsurface counterparts*. The three energy-injection scales correspond reasonably to interior-model convective mixing lengths for H I, He I, and He II 50% ionization depths, respectively. The two larger scales are nearly one-to-two also suggestive of a possible resonant overtone structure. The horizontal supergranulation flow seems evident as a distinct scale of eddy noise without energy injection around wavelength 45.3 Mm, consistent with the first subharmonic of the supergranular subsurface counterpart.

keywords: convection - turbulence - Sun: granulation - Sun: interior - Sun: photosphere

1 Introduction

Granulation and supergranulation are cellular flow patterns seen at the solar surface, which have long been believed to be evidence of deeper convective motions. They have very disparate physical parameters with granulation of scale 1 Mm, lifetime 8 minutes, and velocity 1 km/s, and supergranulation 35 Mm, lifetime 20 hr, and velocity 300 m/s (Hart, 1956; Leighton, Noyes, and Simon, 1962).

Evolutionary models predict a convection zone in the outer 200 Mm of the sun, but theoretical views differ greatly regarding what might be expected for the depth distribution of the convective flows (see review Spruit, 1997). Mixing-length models suggest that convective motions should be strongest within 20 Mm of the solar surface, associated with the H I, He I, and He II ionizations (Stix, 2002). The density scale height in the H I ionization zone is about 1 Mm consistent with the scale of granulation, however, the supergranulation scale exceeds by more than a factor of 3 that expected for convection in the He I or He II ionization zones where density scale heights corresponding roughly to model mixing lengths are less than 10 Mm, as pointed out in many studies (Simon and Leighton, 1964; Simon and Weiss, 1968; Schwarzschild, 1975; Weiss, 1976; Bushby and Favier, 2014). A 35 Mm density scale height is reached only at a depth of 60 Mm.

Supergranulation differs greatly from granulation too as it is very anisotropic, exhibiting a much larger horizontal than vertical velocity, as is evident by the conspicuous absence of signal at the center of the solar disk where steady vertical velocity should be seen in full-disk time-averaged Doppler line-of-sight velocity images like those obtained by Leighton and coworkers.

Long (45-90 minute) time-average Dopplergrams at disk center do reveal a small persistent signal, about one tenth the amplitude of the horizontal supergranulation velocity seen toward the limb (November *et al.*, 1981, hereafter N81) (Kueveler, 1983, Figure 1a–d). The long-lived vertical velocity takes the form of up- and down-welling plumes suggestive of deeper vertical convective motions. However most of the power is in coherent plumes 5–10 Mm in size reported in N81 as 'the scale of change in sign' or half wavelength, much smaller than the ≃35 Mm scale of the supergranulation. N81 suggested that the very different scale might be evidence for a third intermediate convective component, which was called 'mesogranulation'.

Local correlation tracking (LCT) was introduced based upon the Simon (1967) observation that granules appear to be systematically moving on the solar surface toward the supergranulation boundaries, apparently

advected by the supergranulation horizontal flow as they evolve (November, 1986; November *et al.*, 1987; November and Simon, 1988). Since then LCT of granulation has become widely and routinely used in many solar studies. LCT flow maps are more easily obtained without the difficulties due to the strong competing oscillation and granulation velocity signals inherent in Doppler methods.

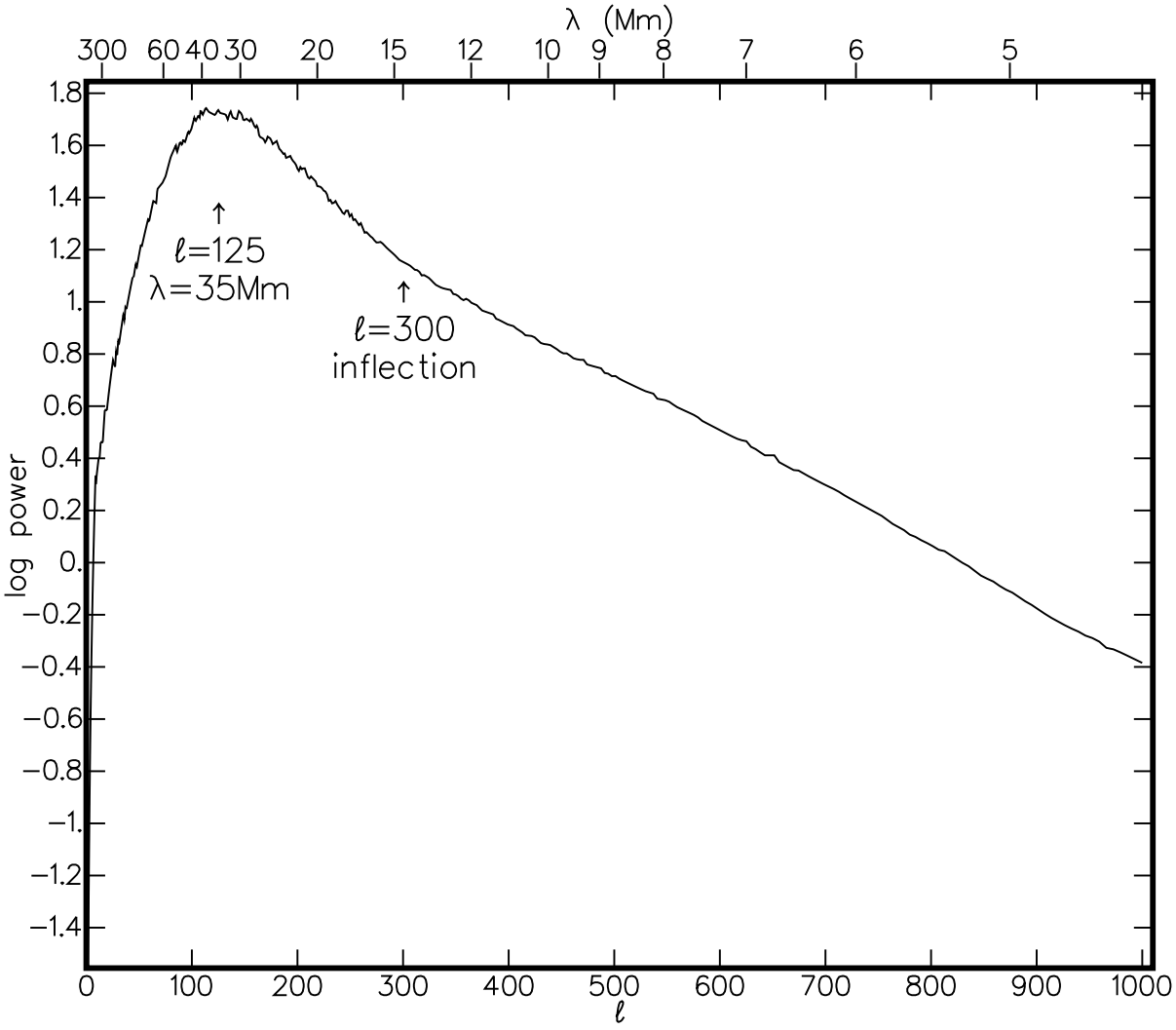

Figure 1: Power spectrum of full-disk long-lived Doppler or horizontal velocity as a function of spherical harmonic ℓ, H00 Figure 3 replotted, with wavelength λ shown on top. The single supergranulation peak at $\ell = 125$ corresponding to $\lambda = 35$ Mm is evident, with no other obvious features that might indicate mesogranulation.

The LCT flow maps show the 2D supergranulation horizontal flow well with mesogranulation too clear as the primary component in the corresponding divergence of the flow, which is a proxy for the vertical velocity. With the local correlation averaged over a number of granulation lifetimes to thoroughly eliminate granulation evolutionary noise, and over many seeing realizations in ground-based observations, signals are found that have proven persistent and reliable, as in the many long time series' that follow the mesogranulation evolution and its systematic motion within the supergranulation network over its several hour lifetime (e.g. Muller *et al.*, 1992; Simon *et al.*, 1994; Shine, Simon, and Hurlburt, 2000).

Much recent work has tried to probe the subsurface using local helioseismology, but very different results seem to suggest that better guidance is needed from surface measurements (Gizon, Birch, and Spruit, 2010). Spectra of the long-lived photospheric Doppler velocity field have been obtained to try to clarify the relation between supergranulation and mesogranulation, like the example shown in Figure 1 taken from Hathaway *et al.* (2000)(hereafter H00), which shows spherical harmonic power from a 31 minute temporally filtered full-disk quiet MDI Dopplergram time series averaged over a 62 day continuous data stream (Domingo, Fleck, and Poland, 1995; Scherrer *et al.*, 1995). H00 show that the temporal filtering is effective in eliminating oscillatory and granulation signals.

The spectrum shows a clear peak around spherical harmonic $\ell = 125$, corresponding to horizontal wavenumber $k = (\ell(\ell+1))^{1/2}/R_\odot = 0.18$ radians/Mm, or wavelength $\lambda = 2\pi/k = 35$ Mm consistent with the scale of supergranulation. As some authors have pointed out from such analyses, there is no other feature in the full-disk long-lived Doppler-velocity spectrum that might indicate a separate mesogranulation scale of motion (H00) (Chou *et al.*, 1991; Straus, Deubner, and Fleck, 1992; Rieutord *et al.*, 2000).

There is a dipping inflection in the curve at $\ell = 300$ corresponding to wavelength 14.6 Mm or half wavelength 7.3 Mm right in the middle of the mesogranulation range, and a long tail in power extending out to much higher wavenumber. Ginet and Simon (1992) contend that the extended range seen in such spectra cannot be accounted for except with the presence of mesogranulation size flows.

The mesogranulation signal is small compared to that of the supergranulation, and evident in the long-lived *vertical* velocity (center-disk Doppler or LCT divergence), whereas the spectrum of Doppler velocity over the full solar disk is essentially determined by the *horizontal* velocity due to its much larger amplitude. November (1994) (hereafter N94) shows that the steady photospheric vertical-velocity spectrum is uniquely determined from the horizontal-velocity spectrum, and an example shown there demonstrates how very different the two may appear. The derived vertical-velocity spectrum is actually superior to the direct spectrum of vertical Doppler velocity because of the much larger horizontal velocity signal and full-disk areal coverage. In this paper, the spectrum of the long-lived vertical velocity is similarly derived from the H00 62 day average Doppler-velocity spectrum shown in Figure 1. The H00 spectrum seems to be the highest quality long-lived large-scale Doppler velocity spectrum available.

2 The Vertical-Velocity Spectrum

The long-lived vertical velocity u_z on the (x, y) solar surface is related to the horizontal velocity (u_x, u_y) through the steady continuity relation

$$\nabla\cdot(\rho\mathbf{u}) = 0, \tag{1}$$

for the vector velocity $\mathbf{u} = (u_x, u_y, u_z)$ in a density ρ. Density variations in a medium of relatively small density scale height are determined mainly by the stratification $\rho \simeq \rho_0(z)$ (November *et al.*, 1987; November, 1989; Simon and Weiss, 1989), giving

$$-\frac{1}{\rho_0(z)}\frac{\partial}{\partial z}\Big(\rho_0(z)u_z\Big) = \frac{\partial u_x}{\partial x} + \frac{\partial u_y}{\partial y}. \tag{2}$$

Expanding the z derivative and substituting with $\partial\rho_0/\partial z = -\rho_0(z)/H_\rho$ and $\partial u_z/\partial z = -u_z/H_{uz}$, definitions for the density scale height H_ρ and vertical-velocity scale height H_{uz}, respectively, then leads to the proportionality between the vertical velocity and horizontal-flow divergence

$$u_z = H_{\rm mf}\left(\frac{\partial u_x}{\partial x} + \frac{\partial u_y}{\partial y}\right), \tag{3}$$

with the proportionality constant the combined scale height for the total mass flux defined

$$\frac{1}{H_{\rm mf}} = \frac{1}{H_\rho} + \frac{1}{H_{uz}}. \tag{4}$$

A reasonably uniform mass-flux scale height $H_{\rm mf} = 125$ km is found over the field of view comparing vertical Doppler velocity and LCT horizontal flow divergence maps (N94). The value $H_{\rm mf} = 125$ km is also

the photospheric density scale height H_ρ, so the vertical-velocity scale height must be much larger than the density scale height in amplitude $|H_{uz}| \gg H_\rho$, for its effect to be negligible in the sum Eq. (4). The vertical velocity u_z may be increasing with height in the solar atmosphere with $H_{uz} < 0$.

The density scale height is smallest and constant within 15% in the solar atmosphere and an increasing function of depth into the solar interior, as illustrated in Figure 5 of N94. Thus a vertical flow must be significantly turned in the small density scale height of the photosphere as suggested in N94. However the horizontal flow may remain large with depth and changing in character, as the vertical-velocity can be large below with its scale height, which may vary horizontally, becoming dominant $|H_{uz}| \lesssim H_\rho$. With a number of different helioseismic inversions, a coherent diverging supergranulation horizontal flow is identified within about 5 Mm of the solar surface, below which the signal may attenuate, flip sign, or noise effects become dominant (Sekii *et al.*, 2007; Woodard, 2007; Jackiewicz, Gizon, and Birch, 2008; Duvall, Hanasoge, and Chakraborty, 2014). Greer, Hindman, and Toomre (2016) report strong horizontal flows of supergranular and larger scale down to 25 Mm solar depth, which are correlated with the surface pattern with a time lag, which suggests the surface horizontal flow slowly drifts downward.

The vertical component of the flow vorticity is defined

$$\omega_z = \frac{\partial u_y}{\partial x} - \frac{\partial u_x}{\partial y}, \tag{5}$$

and the spatial Fourier transforms, denoted by overbars as complex functions of the 2D wavenumber (k_x, k_y), are written with Eq. (3) as

$$\begin{aligned} \bar{u}_z &= -iH_{\rm mf}\left(k_x\bar{u}_x + k_y\bar{u}_y\right), \\ \bar{\omega}_z &= -i\left(k_x\bar{u}_y - k_y\bar{u}_x\right). \end{aligned} \tag{6}$$

Combining gives the power spectrum of the vertical velocity $|\bar{u}_z|^2 = \bar{u}_z\bar{u}_z^*$ from that of the horizontal velocity $|\bar{\mathbf{u}}_{\rm h}|^2 = |\bar{u}_x|^2 + |\bar{u}_y|^2$, as

$$|\bar{u}_z|^2 + H_\rho^2|\bar{\omega}_z|^2 = k^2H_\rho^2|\bar{\mathbf{u}}_{\rm h}|^2, \tag{7}$$

with the horizontal wavenumber defined $k = (k_x^2 + k_y^2)^{1/2}$ in units of radians per Mm, and taking $H_{\rm mf} = H_\rho$ good in the photosphere.

Mostly the mesogranulation-scale vorticity $\omega_{\rm z}$ is observed to be small except at exceptional locations and only for relatively short periods (Simon *et al.*, 1994; Darvann, 1994). Vortices have roughly half the amplitude of divergence elements $\omega_z = (u_z/H_\rho)/2$ and so 1/4 the power and about 1/30 the average areal coverage, making their relative total power less than 1% (comparing Figures 3 and 4 in Simon *et al.*, 1994). Small vortices are also seen in intergranular lanes associated with magnetic elements (Bonet *et al.*, 2008). However because the total area covered by magnetic elements is very small, these make an even much smaller contribution to the total vorticity power. It thus seems justified to ignore vertical vorticity power $|\bar{\omega}_z|^2$ compared to divergence power $k^2|\bar{\mathbf{u}}_{\rm h}|^2$ in Eq. (7), which gives a power spectrum for the steady vertical velocity that goes simply as the spectrum of the horizontal velocity multiplied by horizontal wavenumber k^2, like that explored in N94. The spectral relation Eq. (7) for a negligible vorticity generalizes straightforwardly to spherical harmonics, as elaborated in Appendix A.

Figure 2 portrays the power spectrum of the long-lived vertical velocity (solid line) as a function of spherical harmonic ℓ, that is the H00 Doppler-velocity spectrum from Figure 1 multiplied by $k^2H_\rho^2 = \ell(\ell+1)(H_\rho/R_\odot)^2$. The H00 spectrum is also reproduced (dashed line) in the figure vertically shifted for comparison.

The spectrum of long-lived vertical velocity differs markedly from that of the horizontal. The slow falloff in the horizontal-velocity spectrum beyond its peak at $\ell = 125$ gives a peak shifted to larger wavenumber and considerably broadened with the k^2 or $\ell(\ell+1)$ scaling. The broad peak in the power spectrum of vertical velocity (solid line) ranges from $\lambda/2 = 4$–12 Mm, slightly larger than the 5–10 Mm range of plume sizes reported for mesogranulation in N81.

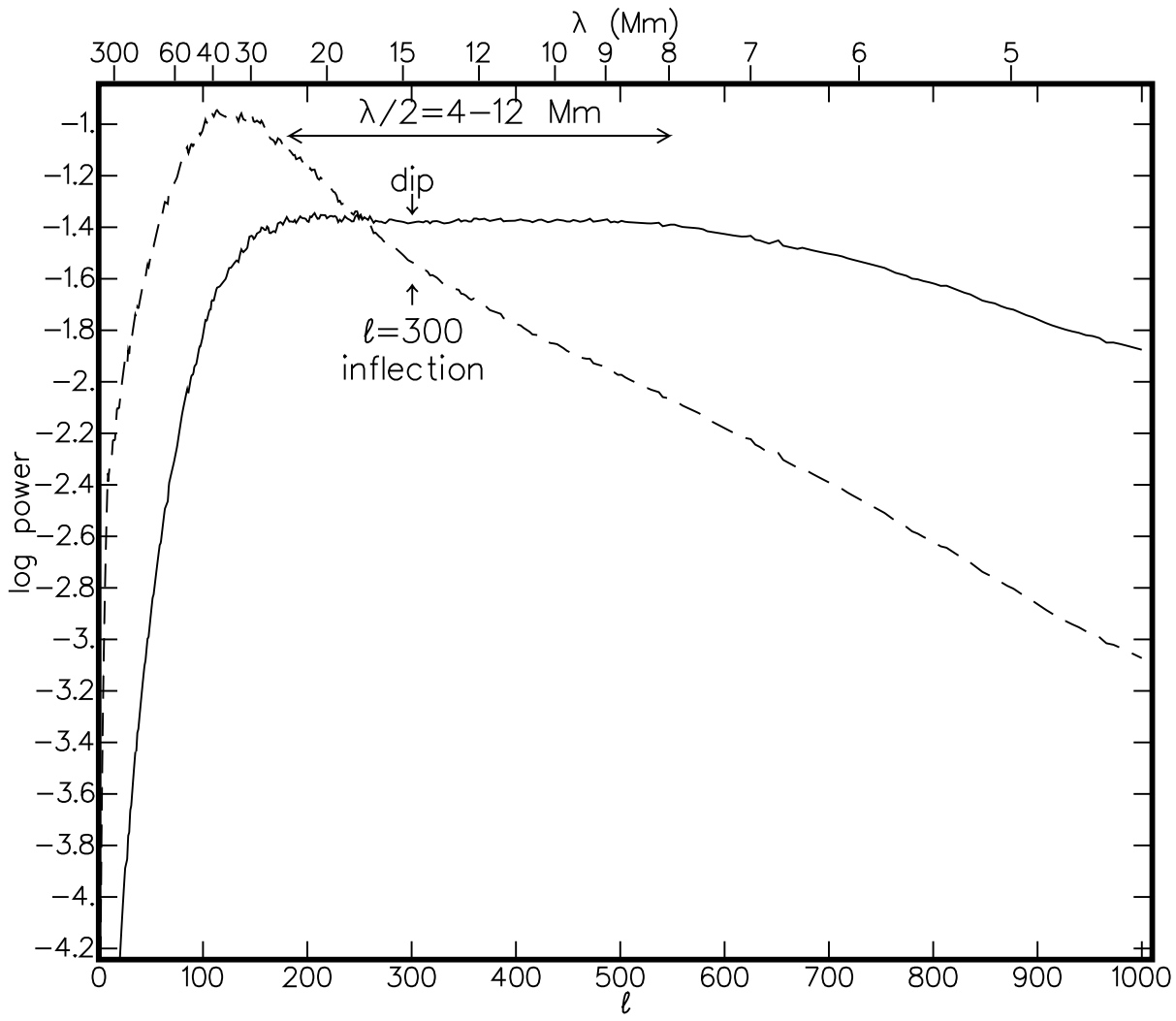

Figure 2: Power spectrum of long-lived vertical velocity (solid line), that is the power spectrum of the horizontal velocity Figure 1 (dashed line) scaled by k^2 or $\ell(\ell+1)$ as a function of spherical harmonic ℓ, with the corresponding wavelength λ shown on top. The peak of the vertical-velocity spectrum is considerably displaced to higher wavenumbers and smaller spatial scale and broadened from that of the horizontal velocity consistent with mesogranulation.

3 The Granulation Spectrum

A single good quality snapshot as obtained using frame selection methods can be sufficient to ascertain the granulation spatial power spectrum. The Koutchmy (1994) (hereafter K94) spectrum of granulation intensity shown in Figure 3 is from IR continuum at 1.6μm made from fast linear scans corrected using a point spread function of the telescope and atmosphere derived from concurrent limb profiles from the SP National Solar Observatory (NSO) Dunn 0.7m vacuum tower telescope.

The K94 spectrum is shown along with a number of other published spectra from: Leighton (1963) (L63, dashed line), Deubner and Mattig (1975) (DM75, dot-dot-dashed line), von der Luhe and Dunn (1987) (vdLD87) obtained by image deconvolution methods (dot-dashed line), and H00 Figure 9 of granulation

velocity (H00g, solid line).

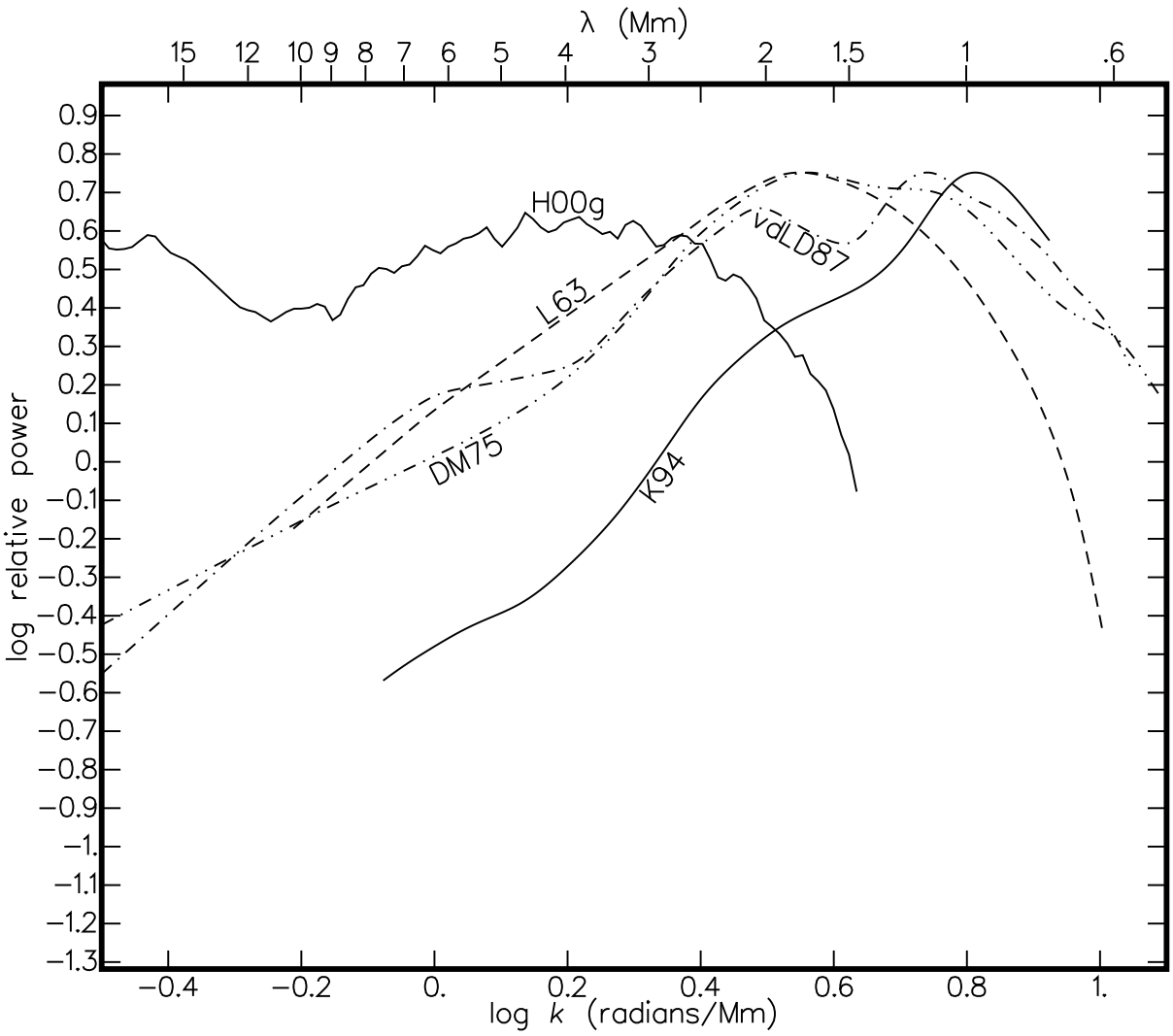

Figure 3: Granulation power spectra from K94 (solid line), and others.

The H00g spectrum shows a rapid falloff around $\lambda = 2$ Mm at the scale where the other granulation spectra are turning on, but consistent with the MDI Airy-disk diameter of 1 Mm and spatial sampling of 0.45 Mm. It shows added power going back to small wavenumbers or wavelengths $\lambda \simeq 10$ Mm into the mesogranulation and supergranulation range, undoubtably due to a relatively small low-wavenumber residual in the granulation spectrum, which seems effectively eliminated in the temporally filtered H00 spectrum of full-disk Doppler velocity Figure 1. The H00g spectrum is made from Doppler velocity, whereas all the other spectra shown are from intensity. The granulation vertical velocity is known to be well correlated with intensity at the deepest photospheric levels, but its horizontal velocity exhibits a larger spatial scale (Beckers and Morrison, 1970).

Granulation may exhibit a small anisotropy between its horizontal and vertical velocities and the long-lived mesogranulation-supergranulation flow field much more. The continuity-derived spectral relation Eq.

(7) for small vorticity is integrated over the range of wavenumbers k to give

$$\int |\bar{u}_z|^2 \pi dk^2 = H_\rho^2 \int k^2 |\bar{\mathbf{u}}_\mathrm{h}|^2 \pi dk^2 = \tilde{k}^2 H_\rho^2 \int |\bar{\mathbf{u}}_\mathrm{h}|^2 \pi dk^2, \tag{8}$$

written for the small density scale height of the photosphere where $H_\mathrm{mf} \simeq H_\rho$, and for radially symmetric spectra in 2D wavenumber with $\pi dk^2 = 2\pi k dk$. A predominant wavenumber $\tilde{k}^2$ is factored out from under the integral in the rightmost equality, which is valid if the horizontal-velocity spectrum $|\bar{\mathbf{u}}_\mathrm{h}|^2$ is sharply peaked around that wavenumber. However the rightmost equality can be seen to remain valid for any well-behaved horizontal-velocity spectrum with the predominant wavenumber *defined* as

$$\tilde{k}^2 = \frac{\int k^2 |\bar{\mathbf{u}}_\mathrm{h}|^2 \pi dk^2}{\int |\bar{\mathbf{u}}_\mathrm{h}|^2 \pi dk^2}. \tag{9}$$

The RMS is the square root of the spatial average $\langle u^2 \rangle = (\int |\bar{u}|^2 \pi dk^2)/A$, applying the Fourier power theorem with the observing area A, which allows the RMS ratio for the flow anisotropy to be written from Eq. (8)

$$a = \frac{\langle \mathbf{u}_\mathrm{h}^2 \rangle^{1/2}}{\langle u_z^2 \rangle^{1/2}} = \frac{1}{\tilde{k} H_\rho}. \tag{10}$$

The deep photospheric granulation intensity spectrum in Figure 3 can be taken as a proxy for vertical velocity. The predominant granulation wavenumber $\tilde{k}$ might be derived using the spectral ratios Eq. (9), except that without very good low-wavenumber information, the translation to horizontal velocity tends to diverge there giving $\tilde{k}$ overestimated beyond the spectral peak. Supposing $\tilde{k}$ to be at or a little beyond the peak in the K94 spectrum gives the RMS ratio $a \lesssim 1.2$ in Eq. (10). Granulation velocities are observed to be nearly isotropic with some small excess in the horizontal velocities near optical depth unity (Komm, Mattig, and Nesis, 1991, Figure 5). The vertical velocity RMS falls to about 500 m/s around $z = 200$ km above optical depth unity.

Integrating numerically in the long-lived supergranulation horizontal velocity spectrum Figure 1, gives a predominant wavenumber $\tilde{k}$ in Eq. (9) corresponding to wavelength $2\pi/\tilde{k} = 8.2$ Mm , which is a little beyond the broad peak in the vertical-velocity mesogranulation spectrum Figure 2. Using the photospheric density scale height $H_\rho = 125$ km then gives the RMS ratio $a = 10.4$ from Eq. (10). The range of mesogranulation Doppler velocity reported in N94 is ± 28 m/s corresponding to RMS $\langle u_z^2 \rangle^{1/2} = 20$ m/s at about $z = 250$ km for near half depth in the Fe I 5576Å line (Altrock *et al.*, 1975). Compared to a horizontal supergranulation velocity RMS of $\langle \mathbf{u}_\mathrm{h}^2 \rangle^{1/2} = 300$ m/s around that height, the 20 m/s vertical RMS implies the anisotropy ratio $a \simeq 15$. Hathaway *et al.* (2002) report a slightly larger RMS for the long-lived vertical Doppler velocity of 29 m/s and a smaller horizontal RMS of 258 m/s at the deeper atmospheric height of 200 km for the MDI measurement giving the somewhat smaller anisotropy ratio $a \simeq 9$.

The N81 mesogranulation measurement of 60 m/s RMS sampled the temperature minimum region where granulation vertical velocities die out and the larger-scale overshooting convective flows are enhanced. Granulation represents a noise contribution to horizontal Doppler velocity, but a much more significant noise contribution to the directly measured long-lived vertical Doppler signal from sun-centered measurements. Intensity patterns associated with both mesogranulation and supergranulation scales are even seen in Lyα intensity in the upper chromosphere (Kariyappa, Varghese, and Curdt, 2001). [1]

4 The Convective Power Spectrum

The long-lived vertical-velocity spectrum is reproduced in Figure 4 with the granulation K94 spectrum on scales of common log wavenumber and log power for about $z = 200$ km above optical depth unity, taking granulation intensity to be a proxy for vertical velocity. Of the granulation spectra shown in Figure 3, K94 sees the finest scales, and shows the most consistent convective signature.

[1] Usually the large oscillation signal easily averages out, but if the the spectral line is not tracked, as in measurements obtained with a nontunable filter, then a nonlinear residual non-persistent signal with the scale of mesogranulation can be left.

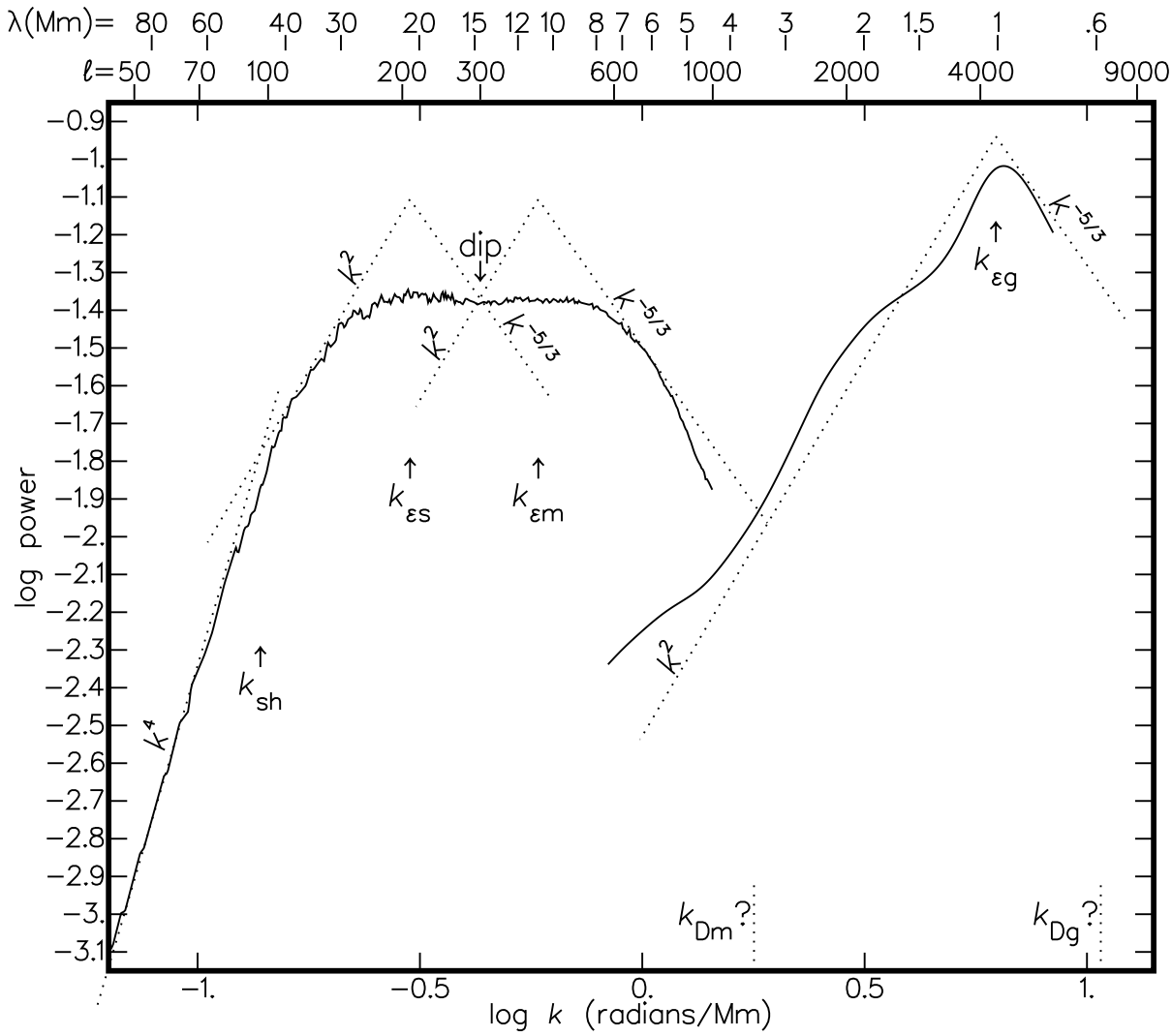

Figure 4: The long-lived vertical-velocity spectrum derived from the H00 Doppler-velocity spectrum and the granulation spectrum from K94 as functions of $\log(k)$. The spectra show characteristic Kolmogorov inertial and eddy-noise subranges at wavenumbers larger and smaller, respectively, than energy-injection wavenumbers.

Kolmogorov inertial subranges are evident in both spectra falling off as $k^{-5/3}$ at wavenumbers greater than energy-injection wavenumbers $k_{\epsilon\mathrm{m}}$ and $k_{\epsilon\mathrm{g}}$. A Kolmogorov inertial subrange has been inferred before in spatio-temporal analyses of granulation (Espagnet *et al.*, 1993), and mesogranulation (Muller *et al.*, 1987; Ruzmaikin *et al.*, 1996).

A slight tailing off in power below both $k^{-5/3}$ lines approaching wavenumbers $k = k_{\mathrm{Dsm}}$ and k_{Dg} might seem to suggest some change in the character of the turbulence approaching wavenumber cutoffs. In classical turbulence theory, such cutoffs arise due to eddy viscosity with effective turbulent-eddy Reynolds' numbers defined by the ratios $R_{\mathrm{m}} = (k_{\mathrm{Dm}}/k_{\epsilon\mathrm{m}})^{4/3}$ =4.3, $R_{\mathrm{g}} = (k_{\mathrm{Dg}}/k_{\epsilon\mathrm{g}})^{4/3}$ =2.1, which seem rather small for Reynolds' numbers associated with solar convective instabilities. Rather the full wavenumber extent of mesogranulation and granulation appears to be artificially limited by the resolutions of the observations. With an effective Reynolds' number as small as 30, convection is linear and well-described by the mixing-

length approximation (Unno, 1961).

The rise in power leading up to energy-injection wavenumbers obeys the well-known k^2 power law below energy-injection wavenumbers at $k_{\epsilon s}$ and $k_{\epsilon g}$. A k^2 low-wavenumber extension is commonly seen in laboratory turbulence, arising due to interference between turbulent eddies of similar scale, 'eddy noise', at energy-injection wavenumbers (Rose, 1977; Pouquet, Frisch, and Chollet, 1983; Frisch, 1995).

The broad peak in the long-lived vertical-velocity spectrum hints at a dip corresponding to the well-defined inflection in the horizontal-velocity spectrum at $\ell = 300$ in Figures 1 and 2. Falling power for $k > k_{\epsilon s}$ along a $k^{-5/3}$ power law and rising power for $k < k_{\epsilon m}$ along a k^2 power law, are illustrated crossing in the dip, which locate the central energy-injection wavenumbers $k_{\epsilon s}$ and $k_{\epsilon m}$. Energy appears to be being pumped in around the two separate wavelengths 21 Mm and 10.8 Mm corresponding to plume sizes of 10.5 Mm and 5.4 Mm, giving possible evidence for two predominant subphotospheric convection scales.

The spectral k^4 power rise changes rather quickly into a k^2 power law at $k_{\rm sh}$ leading into the energy-injection wavenumber $k_{\epsilon s}$. That power rise is consistent with eddy noise in the horizontal flow field (the spectrum of vertical velocity divided by k^2) around $\ell = 96$ or wavelength $\lambda = 45.3$ Mm. No energy injection is evident in the photospheric spectrum at $k_{\rm sh}$ as no inertial subrange follows at higher wavenumber.

The long-lived vertical-velocity and granulation spectra are shown on a common scale of power, supposing a 17 fold increase in the granulation RMS velocity compared to the long-lived vertical velocity, which is about right for $z = 200$ km. At deeper levels in the atmosphere, the relative granulation signal is larger. The relative units of power are arbitrary as are the observing areas, but by the Fourier power theorem, power levels scale upward with the squared RMS signal and downward with the area under the spectral curve in 2D horizontal wavenumber k, allowing the granulation curve to be vertically shifted to correspond to the 17 fold ratio of RMS signals. Numerical integrals under the power curves are taken from a low wavenumber to beyond the projected cutoffs $k_{\rm Dm}$ and $k_{\rm Dg}$, but the exact range is not critical. Though it appears smaller in projection, the area under the granulation spectrum is actually much larger than that of the long-lived vertical-velocity spectrum in 2D horizontal wavenumber, as it sweeps out a larger k annulus in (k_x, k_y).

5 Discussion

In a stratified medium of relatively small density scale height, the vertical component of the steady velocity is everywhere proportional to the divergence of the horizontal, with the constant of proportionality the density scale height. The proportionality is validated for the long-lived solar flow in N94 comparing simultaneous disk-center Doppler maps with LCT horizontal-flow divergences.

Where the vertical vorticity is also small, the spectrum of vertical velocity is that of the horizontal times the horizontal wavenumber k^2. While the spectrum of the long-lived horizontal velocity in Figure 1 shows a clear peak at wavelength 35 Mm, 'supergranulation', the derived spectrum of vertical velocity in Figure 2 shows a broad divided peak with a range of half wavelengths 4–12 Mm, 'mesogranulation'. The spectral relation leads to a relative anisotropy ratio of horizontal to vertical RMS that increases roughly in proportion to the horizontal scale of the vertical flow component, $\lesssim$1.2 for granulation and 10.4 for the long-lived mesogranulation-supergranulation flow field, consistent with observations.

Solar photospheric steady vertical-velocity spectra for both granulation and the long-lived flow conform to classical Kolmogorov theory, suggesting that those spectra retain signatures of convective flows coming from below within the solar interior. On the other hand, the horizontal velocity corresponds to the deflected vertical velocity in the thin photosphere. By mass continuity, vertical plumes feed a larger-scale larger-amplitude horizontal surface flow as an integrating effect, rather than producing a pattern of closed 3D cells. The Kolmogorov spectral features identified in the vertical-velocity spectrum become quite subtle inclination deviations, and while still present, are easily missed or misinterpreted in the corresponding horizontal-velocity spectrum.

The broad top in the long-lived vertical-velocity mesogranulation spectrum in the range of half wavelengths of 4–12 Mm is a little larger than the range of scales 5–10 Mm reported in N81. Extensions to both smaller and larger wavenumber corresponding to eddy-noise and Kolmogorov inertial subranges, respectively, seem suggested as well. Observations do report a considerable range of scales for mesogran-

ulation, perhaps even overlapping in size with the much shorter-lived granulation (Dialetis *et al.*, 1988; Straus, Deubner, and Fleck, 1992) (cf. Lawrence, Cadavid, and Ruzmaikin, 2001). Persistent mesogranulation scales of motion are seen in some spatial spectra made using Doppler observation or analysis methods that may have increased sensitivity to the vertical flow (Chou *et al.*, 1992; Ruzmaikin *et al.*, 1996).

Though related to supergranulation, mesogranulation exhibits morphologically distinct features: Granules systematically change with scale $\simeq$8 Mm suggesting that they are distorted at convergence and divergence sites in their advection on the steady horizontal flow (e.g. Oda, 1984; Title *et al.*, 1989; Abdussamatov, 2000). The changing granulation pattern may be consistent with the reported >4 Mm systematic variation seen in the photospheric temperature contrast (Koutchmy and Lebecq, 1986). It has been suggested that granulation may arise as a secondary near-surface instability of the subphotospheric mesogranulation flow (Getling, 2000) (cf. Roudier and Muller, 2004).

Simon and Weiss (1989) trace the motion of 'corks' in the 2D LCT-measured surface flow showing first their accumulation in the downflow sites in the smaller vertical 4–12 Mm plumes, and then their eventual relocation to the 35 Mm stagnation points of the horizontal flow, consistent with the small-scale magnetic network seen in active regions where the rate of flux emergence is high and the 35 Mm quiet sun network where it is low. Small magnetic elements are seen preferentially in the mesogranulation downflows (Roudier *et al.*, 1997; Domínguez Cerdeña, 2003; de Wijn *et al.*, 2006; Requerey *et al.*, 2017), with magnetic fields mainly horizontal at downflow sites with horizontal flow, and vertical near the supergranulation boundaries where horizontal flows stagnate (Ishikawa and Tsuneta, 2010). A smaller 13-18 Mm average size of chromospheric network is found using pattern recognition rather than autocorrelation methods of analysis (Hagenaar, Schrijver, and Title, 1997).

The Deubner (1989) intensity-velocity correlation seen at the intermediate mesogranulation scale is suggestive of a convective signature still in evidence for flows driven near the solar surface. Mesogranulation appears to rotate slower than supergranulation, which may suggest that the flow fields originate at differing depths (Rast, Lisle, and Toomre, 2004). Vertical plumes of 5–10 Mm size are inferred at least down to 2 Mm below the solar surface using helioseismology (Woodard, 2009).

Since they are vertical and horizontal components of the same velocity field, November (1989) suggested, that 'mesogranulation' might rather have been called 'the principle component of the vertical velocity' of the overall supergranulation flow field. However a divided peak in the vertical-velocity spectrum in evidence in this work, may suggest two preferred scales of turbulent energy injection from below around plume sizes of 5.4 Mm and 10.5 Mm shown in Figure 4, referred to here as 'mesogranular' and 'supergranular' *subsurface counterparts*.

In the following table, relevant horizontal coherence scales d are listed with depths $-z$ below optical depth unity, temperatures T, and density and pressure scale heights H_ρ and H_P, at species-ionization depths. Parameters are taken from a helioseismic-calibrated solar mixing-length convection-zone model (Christensen-Dalsgaard *et al.*, 1996) where it crosses temperature-density curves for 50% ionization from stellar solutions to the Saha ionization formula (Menzel, Bhatnagar, and Sen, 1963, Section 3.5).

	H I	He I	He II
depth $-z$	2.23 Mm	7.96 Mm	17.08 Mm
T	19.6E3K	52.9E3K	124.0E3K
H_ρ	0.814 Mm	3.47 Mm	8.78 Mm
H_P	0.651 Mm	2.33 Mm	5.51 Mm
component	granulation	mesogranular	supergranular
RMS $\langle u_z^2 \rangle^{1/2}$	500 m/s	26 m/s	13 m/s
wavelength λ	1.01 Mm	10.8 Mm	21.0 Mm
coherence scale d	$\gtrsim$1.01 Mm	5.4 Mm	10.5 Mm
mixing length $\alpha_\rho = d/H_\rho$	$\gtrsim$1.24	1.56	1.20
mixing length $\alpha_P = d/H_P$	$\gtrsim$1.55	2.32	1.91

RMS vertical velocities are for $z = 200$ km atmospheric height, estimated from a total long-lived vertical-

velocity RMS $\langle u^2_{z\mathrm{sm}}\rangle^{1/2} = 29$ m/s from the spatial average $\langle u^2_{z\mathrm{sm}}\rangle = \langle u^2_{z\mathrm{s}}\rangle + \langle u^2_{z\mathrm{m}}\rangle$, supposing that the supergranular and mesogranular subsurface counterparts are spatially incoherent. The wavenumber power spectra for the supergranular and mesogranular subsurface counterparts from Figure 4 are assumed to be identical in form, but with supergranular power shifted to half wavenumber, which gives $\langle u^2_{z\mathrm{s}}\rangle = \langle u^2_{z\mathrm{m}}\rangle/4$, defining the RMS velocity using the Fourier power theorem. Undoubtably the flows that are seen are overshooting motions carrying energy-injection signatures from below, with relative strengths that may vary a little with height in the atmosphere, but much more with depth, especially in passing into or through their possibly separate regions of strong convection.

Coherence scales d for granulation, mesogranular, and supergranular subsurface counterparts are defined based upon their energy-injection wavelengths λ. A coherence scale of half the wavelength $d = \lambda/2$ for the mesogranular and supergranular subsurface counterparts best matches mesogranulation plume cross sections (N81) (Simon and Weiss, 1989, Figure 10b). Granulation gives evidence for spatial coherence on its full wavelength scale $d = \lambda$ due to its rather more consistent asymmetric appearance as a broad upflow surrounded by downflow in narrow lanes. Actually the coherence scale for granulation may be larger than its principle wavelength $d \gtrsim \lambda$, as granules appear to be tightly packed, suggesting that their spatial separation may be smaller than their coherent plume size.

All three energy-injection eddy sizes have mixing-length ratios of coherence length to pressure scale height reasonably close to $\alpha_P = d/H_P = 2$, consistent with the most optimum mixing length found in the fit of the standard solar model with helioseismic inverses (Christensen-Dalsgaard *et al.*, 1996). Convective scales deviate near convection-zone boundaries adding to the uncertainty in the granulation comparison (Deupree, 1979). Other solar models with somewhat smaller mixing lengths $\alpha_P = 1.75$ give a better match to Li abundances and may better predict consistent solar neutrino fluxes (Guzik *et al.*, 2001). The very near two-to-one ratio between the central energy-injection wavenumbers for the mesogranular and supergranular subsurface counterparts actually seems more consistent with a resonant convective overtone structure, originating around one depth as in the convection models of Toomre, Gough, and Spiegel (1982), or two depths.

Observations have suggested multiple convective components as Getling and Buchnev (2010), who distinguish exceptional 15 Mm mesogranules apart from normal 5–10 Mm mesogranulation and the supergranulation horizontal flow pattern. Observations of smaller plumes advected by larger-scale horizontal flows (Muller *et al.*, 1992; Shine, Simon, and Hurlburt, 2000; Leitzinger *et al.*, 2005) may discriminate between distinct subsurface components. Ustyugov (2008) reports similar discrete scales in solar convection-zone simulations.

No direct convective energy input with the larger supergranulation horizontal flow scale is seen in the power spectrum Figure 4, but the clear inflection at $\lambda = 45.3$ Mm is indicative of a distinct scale of eddy noise in the horizontal flow field. That scale is about 26% larger than the 35 Mm scale for the horizontal supergranulation flow as defined by the peak in the power spectrum of Figure 1. Actually the peak surface scale for the horizontal flows lies in the eddy-noise subrange of the He II supergranular subsurface counterpart.

The long-lived horizontal flow must have a larger spatial scale than the vertical flow in the small density scale height of the photosphere. The horizontal eddy size of 45.3 Mm is a little larger than 4 times the plume size or twice the wavelength, and so may be the first subharmonic in the He II plume distribution. Subharmonics should be selected as upflows and downflows from the larger-scale horizontal eddies must still be delineated by the flow pattern of the vertical plumes.

Appendix

A Spherical-Harmonic Power Spectra

The vertical-horizontal velocity relation of Eqs. (1) – (3) generalizes to global spherical coordinates (R, Θ, Φ) with z going over to radius R from the sun center, and the horizontal gradient ∇_h in (x, y) going over to

(Θ, Φ), spherical colatitude and longitude, written

$$u_R = H_{\rm mf} \nabla_{\rm h} \cdot \mathbf{u}_{\rm h}, \tag{11}$$

for the horizontal velocity vector $\mathbf{u}_{\rm h}$ in (Θ, Φ), with the scale height for the total mass flux as before in Eq. (4) but with scale heights defined here with respect to the radial R coordinate $1/H_\rho = -\partial \ln(\rho_0)/\partial R$, and $1/H_{uR} = -\partial \ln(u_R)/\partial R$.

With zero vorticity in 3D, the velocity is derivable from a potential function, written in its horizontal component as

$$\mathbf{u}_{\rm h} = \nabla_{\rm h} \Upsilon. \tag{12}$$

The vertical velocity is only derived at the solar surface $R = R_\odot$, so no constraint on the depth variation of Υ is imposed. [2] Thus from Eq. (11)

$$u_R = H_{\rm mf} \nabla_{\rm h}^2 \Upsilon. \tag{13}$$

The velocity elements can be decomposed into series' over complex spherical harmonic functions $Y_\ell^m(\Theta, \Phi)$ as

$$\mathfrak{w}(\Theta, \Phi) = \sum_{\ell m} \bar{\mathfrak{w}}_{\ell m} Y_\ell^m(\Theta, \Phi), \tag{14}$$

counting from $\ell \geq 0$ and $-\ell \leq m \leq \ell$, and using $\mathfrak{w}$ to denote any of the scalar or vector quantities at a given radial height R. Substituting spherical harmonic series' for u_R and Υ as sums over ℓ' and m' in Eq. (13), multiplying through by the conjugate $Y_\ell^m(\Theta, \Phi)^*$, and integrating over the surface of the sphere S in colatitude from $0 \leq \Theta \leq \pi$ and in longitude from $0 \leq \Phi \leq 2\pi$ in the surface element $dS = 2\pi R \sin\Theta \, d\Phi R d\Theta$, gives

$$\bar{u}_{R\ell m} = H_{\rm mf} \sum_{\ell' m'} \bar{\Upsilon}_{\ell' m'} \int_S Y_\ell^{m*} \nabla_{\rm h}^2 Y_{\ell'}^{m'} \, dS = \frac{\ell(\ell+1)}{R^2} H_{\rm mf} \bar{\Upsilon}_{\ell m}, \tag{15}$$

using the orthonormal properties of the Y_ℓ^m functions in the integration on the left side of the first equality $\int_S Y_\ell^{m*} Y_{\ell'}^{m'} \, dS = \delta_{\ell\ell'} \delta_{mm'}$ in terms of Kronecker deltas, and evaluating the well-known orthogonal angular-momentum projection integral from quantum mechanics $\int_S Y_\ell^{m*} \nabla_{\rm h}^2 Y_{\ell'}^{m'} \, dS = \ell(\ell+1) \delta_{\ell\ell'} \delta_{mm'}/R^2$ across the second equality.

Expanding the horizontal velocity vector $\mathbf{u}_{\rm h}$ and the potential Υ in Eq. (12) as spherical harmonic series' in ℓ', m', dotting them with their conjugates as series' in ℓ, m, and integrating the product over the spherical surface S at radius R gives

$$\sum_{\ell m} |\bar{\mathbf{u}}_{\rm h \ell m}|^2 = \sum_{\ell m} \sum_{\ell' m'} \bar{\Upsilon}_{\ell m} \bar{\Upsilon}^*_{\ell' m'} \int_S (\nabla_{\rm h} Y_\ell^{m*}) \cdot (\nabla_{\rm h} Y_{\ell'}^{m'}) dS, \tag{16}$$

having evaluated the integral on the left side of the equality using the orthonormality of the spherical harmonic functions. The integral on the right is also orthogonal as validated using Mathematica (Wolfram, 1991), $\int_S (\nabla_{\rm h} Y_\ell^{m*}) \cdot (\nabla_{\rm h} Y_{\ell'}^{m'}) dS = \ell(\ell+1) \delta_{\ell\ell'} \delta_{mm'}/R^2$, thus giving

$$\sum_{\ell m} |\bar{\mathbf{u}}_{\rm h \ell m}|^2 = \sum_{\ell m} \frac{\ell(\ell+1)}{R^2} |\bar{\Upsilon}_{\ell m}|^2. \tag{17}$$

Since the sums are over arbitrary lists of coefficients for different spherical harmonic power spectra, and any combination of coefficients is possible, the individual ℓ, m terms can be separately equated as

$$|\bar{\mathbf{u}}_{\rm h \ell m}|^2 = \frac{\ell(\ell+1)}{R_\odot^2} |\bar{\Upsilon}_{\ell m}|^2, \tag{18}$$

[2] Without depth information, it is unknown if the horizontal components of the solar vorticity vanish. But even with a vanishing vertical vorticity only, the horizontal potential decomposition of Eq. (12) is still justified, exactly in Cartesian coordinates, cf. Eq. (5), or to within the curvature in spherical coordinates, which is of order $H_\rho/R_\odot \lesssim 2\text{E}{-}4$ in the solar photosphere, still much less than the observed relative vertical vorticity.

which combined with Eq. (15) gives the relation for spherical harmonic power between the radial and horizontal velocity elements

$$|\bar{u}_{R\ell m}|^2 = \frac{\ell(\ell+1)}{R_\odot^2} H_\rho^2 |\bar{\mathbf{u}}_{\mathrm{h}\ell\mathrm{m}}|^2. \tag{19}$$

with both equations written for the solar surface with $R = R_\odot$ and $H_{\mathrm{mf}} = H_\rho$. The spherical harmonic power spectrum of the radial velocity component is directly related to that of the horizontal with the multiplication by $(\ell(\ell+1)/R_\odot^2)H_\rho^2$ as in the Fourier product with $k^2 H_\rho^2$ from Eq. (7).

Strictly, the H00 spectrum is the direct spherical harmonic transform of the long-lived line-of-sight Doppler velocity u_{D} rather than the horizontal velocity $\mathbf{u}_{\mathrm{h}}$. In a dominant horizontal flow, Doppler velocity u_{D} exhibits a unique relationship with the potential function Υ

$$u_{\mathrm{D}} = \mathcal{M}(\Theta,\Phi)(\cos\Theta\sin\Phi, \sin\Theta\cos\Phi)\cdot\nabla_{\mathrm{h}}\Upsilon, \tag{20}$$

projecting velocity on the solar surface $\nabla_{\mathrm{h}}\Upsilon$ in its (Θ,Φ) vector elements into the line-of-sight direction for Doppler velocity u_{D}, taking the center of the visible disk to be at $(\Theta,\Phi) = (\pi/2, \pi/2)$, with a possible mask $\mathcal{M}(\Theta,\Phi)$ commonly applied to avoid Doppler noise near the limb. Expanding u_{D} and Υ as spherical harmonic series' as in Eq. (14), multiplying both sides by $Y_{\ell'}^{m'}(\Theta,\Phi)^*$ and integrating over the facing half disk from $0 \le \Theta \le \pi$ and $0 \le \Phi \le \pi$ where there is data, transforms Eq. (20) into a matrix equation (sparse without the mask) that maps $\bar{\Upsilon}_{\ell m}$ into $\bar{u}_{\mathrm{D}\ell'\mathrm{m}'}$. The measured Doppler velocities analyzed into spherical harmonic components $\bar{u}_{\mathrm{D}\ell'\mathrm{m}'}$ can thus be mapped into $\bar{\Upsilon}_{\ell m}$ with the inverse matrix multiply, which then gives the spectrum of horizontal velocity $|\bar{\mathbf{u}}_{\mathrm{h}\ell\mathrm{m}}|^2$ from Eq. (18) and vertical velocity $|\bar{u}_{R\ell m}|^2$ from Eq. (19) or (7).

Numerical experiments show that introduced (Θ,Φ) dependencies with no mask $\mathcal{M} = 1$ lead to a shift in power from a given (ℓ, m) in $\bar{\Upsilon}_{\ell m}$ to $(\ell+2, m+1)$ and $(\ell-2, m-1)$ in $\bar{u}_{\mathrm{D}\ell'\mathrm{m}'}$. The mapping in m does not produce a systematic change in power in ℓ. Additional 5% power residuals are produced in ℓ at ± 2 intervals, and .07% residuals at ± 4 intervals. The effect of a limb mask is minimal, so the Doppler-velocity spectrum in ℓ reasonably approximates the horizontal-velocity spectrum with a ± 1.5 smearing, an effect that would be difficult to discern in the figures.

References

Abdussamatov, H.I.: 2000, Mesostructure of the Solar Granulation. *Astronomy Letters* **26**, 192. DOI. ADS.

Altrock, R.C., November, L.J., Simon, G.W., Milkey, R.W., Worden, S.P.: 1975, Heights of formation of non-magnetic solar lines suitable for velocity studies. *Solar Phys.* **43**, 33. DOI. ADS.

Beckers, J.M., Morrison, R.A.: 1970, The Interpretation of Velocity Filtergrams. III: Velocities Inside Solar Granules. *Solar Phys.* **14**, 280. DOI. ADS.

Bonet, J.A., Márquez, I., Sánchez Almeida, J., Cabello, I., Domingo, V.: 2008, Convectively Driven Vortex Flows in the Sun. *ApJ* **687**, L131. DOI. ADS.

Bushby, P.J., Favier, B.: 2014, Mesogranulation and small-scale dynamo action in the quiet Sun. *A&A* **562**, A72. DOI. ADS.

Chou, D.-Y., Labonte, B.J., Braun, D.C., Duvall, T.L. Jr.: 1991, Power spectra of solar convection. *ApJ* **372**, 314. DOI. ADS.

Chou, D.-Y., Chen, C.-S., Ou, K.-T., Wang, C.-C.: 1992, Power spectra of median- and small-scale solar convection. *ApJ* **396**, 333. DOI. ADS.

Christensen-Dalsgaard, J., Dappen, W., Ajukov, S.V., Anderson, E.R., Antia, H.M., Basu, S., Baturin, V.A., Berthomieu, G., Chaboyer, B., Chitre, S.M., Cox, A.N., Demarque, P., Donatowicz, J., Dziembowski, W.A., Gabriel, M., Gough, D.O., Guenther, D.B., Guzik, J.A., Harvey, J.W., Hill, F., Houdek, G., Iglesias,

C.A., Kosovichev, A.G., Leibacher, J.W., Morel, P., Proffitt, C.R., Provost, J., Reiter, J., Rhodes, E.J. Jr., Rogers, F.J., Roxburgh, I.W., Thompson, M.J., Ulrich, R.K.: 1996, The Current State of Solar Modeling. *Science* **272**, 1286. DOI. ADS.

Darvann, T.A.: 1994, Measurements of Horizontal Flows in 1.6 μm Granulation. In: Rabin, D.M., Jefferies, J.T., Lindsey, C. (eds.) *Infrared Solar Physics*, *IAU Symposium* **154**, 259. ADS.

de Wijn, A.G., Rutten, R.J., Haverkamp, E.M.W.P., Sütterlin, P.: 2006, Magnetic Patches in Internetwork Areas. In: Leibacher, J., Stein, R.F., Uitenbroek, H. (eds.) *Solar MHD Theory and Observations: A High Spatial Resolution Perspective*, *Astronomical Society of the Pacific Conference Series* **354**, 20. ADS.

Deubner, F.-L.: 1989, Mesogranulation - a convective phenomenon. *A&A* **216**, 259. ADS.

Deubner, F.L., Mattig, W.: 1975, New observations of the granular intensity fluctuations. *A&A* **45**, 167. ADS.

Deupree, R.G.: 1979, Another fundamental, but correctable, inconsistency of the local mixing-length theory. *ApJ* **234**, 228. DOI. ADS.

Dialetis, D., Macris, C., Prokakis, T., Muller, R.: 1988, A possible relation between lifetime and location of solar granules. *A&A* **204**, 275. ADS.

Domingo, V., Fleck, B., Poland, A.I.: 1995, The SOHO Mission: an Overview. *Solar Phys.* **162**, 1. DOI. ADS.

Domínguez Cerdeña, I.: 2003, Evidence of mesogranulation from magnetograms of the Sun. *A&A* **412**, L65. DOI. ADS.

Duvall, T.L., Hanasoge, S.M., Chakraborty, S.: 2014, Additional Evidence Supporting a Model of Shallow, High-Speed Supergranulation. *Solar Phys.* **289**, 3421. DOI. ADS.

Espagnet, O., Muller, R., Roudier, T., Mein, N.: 1993, Turbulent power spectra of solar granulation. *A&A* **271**, 589. ADS.

Frisch, U.: 1995, *Turbulence. The legacy of A. N. Kolmogorov*, Cambridge University Press, Cambridge (UK). ADS.

Getling, A.V.: 2000, Hydrodynamic Instabilities and Photospheric Structures. *Astronomy Reports* **44**, 56. DOI. ADS.

Getling, A.V., Buchnev, A.A.: 2010, Some structural features of the convective-velocity field in the solar photosphere. *Astronomy Reports* **54**, 254. DOI. ADS.

Ginet, G.P., Simon, G.W.: 1992, On the evidence for mesogranules in solar power spectra. *ApJ* **386**, 359. DOI. ADS.

Gizon, L., Birch, A.C., Spruit, H.C.: 2010, Local Helioseismology: Three-Dimensional Imaging of the Solar Interior. *ARA&A* **48**, 289. DOI. ADS.

Greer, B.J., Hindman, B.W., Toomre, J.: 2016, Helioseismic Imaging of Supergranulation throughout the Sun's Near-Surface Shear Layer. *ApJ* **824**, 128. DOI. ADS.

Guzik, J.A., Neuforge-Verheecke, C., Young, A.C., Epstein, R.I., Poulin, F.M., Schissel, J.R.: 2001, Standard and Non-Standard Solar Models. *Solar Phys.* **200**, 305. DOI. ADS.

Hagenaar, H.J., Schrijver, C.J., Title, A.M.: 1997, The Distribution of Cell Sizes of the Solar Chromospheric Network. *ApJ* **481**, 988. DOI. ADS.

Hart, A.B.: 1956, Motions in the Sun at the photospheric level. VI. Large-scale motions in the equatorial region. *MNRAS* **116**, 38. DOI. ADS.

Hathaway, D.H., Beck, J.G., Bogart, R.S., Bachmann, K.T., Khatri, G., Petitto, J.M., Han, S., Raymond, J.: 2000, The Photospheric Convection Spectrum. *Solar Phys.* **193**, 299. DOI. ADS.

Hathaway, D.H., Beck, J.G., Han, S., Raymond, J.: 2002, Radial Flows in Supergranules. *Solar Phys.* **205**, 25. DOI. ADS.

Ishikawa, R., Tsuneta, S.: 2010, Spatial and Temporal Distributions of Transient Horizontal Magnetic Fields with Deep Exposure. *ApJ* **718**, L171. DOI. ADS.

Jackiewicz, J., Gizon, L., Birch, A.C.: 2008, High-Resolution Mapping of Flows in the Solar Interior: Fully Consistent OLA Inversion of Helioseismic Travel Times. *Solar Phys.* **251**, 381. DOI. ADS.

Kariyappa, R., Varghese, B.A., Curdt, W.: 2001, Temporal and spatial variations of the quiet upper chromosphere from SOHO/SUMER observations of hydrogen Lyman lines. *A&A* **374**, 691. DOI. ADS.

Komm, R., Mattig, W., Nesis, A.: 1991, The small-scale velocity field in the solar photosphere. *A&A* **243**, 251. ADS.

Koutchmy, S.: 1994, The Infrared Granulation - Observations. In: Rabin, D.M., Jefferies, J.T., Lindsey, C. (eds.) *Infrared Solar Physics*, *IAU Symposium* **154**, 239. ADS.

Koutchmy, S., Lebecq, C.: 1986, The solar granulation. II - Photographic and photoelectric analysis of photospheric intensity fluctuations at the meso-granulation scale. *A&A* **169**, 323. ADS.

Kueveler, G.: 1983, Velocity fields of individual supergranules. *Solar Phys.* **88**, 13. DOI. ADS.

Lawrence, J.K., Cadavid, A.C., Ruzmaikin, A.: 2001, Mesogranulation and Turbulence in Photospheric Flows. *Solar Phys.* **202**, 27. DOI. ADS.

Leighton, R.B.: 1963, The Solar Granulation. *ARA&A* **1**, 19. DOI. ADS.

Leighton, R.B., Noyes, R.W., Simon, G.W.: 1962, Velocity Fields in the Solar Atmosphere. I. Preliminary Report. *ApJ* **135**, 474. DOI. ADS.

Leitzinger, M., Brandt, P.N., Hanslmeier, A., Pötzi, W., Hirzberger, J.: 2005, Dynamics of solar mesogranulation. *A&A* **444**, 245. DOI. ADS.

Menzel, D.H., Bhatnagar, P.L., Sen, H.K.: 1963, *Stellar Interiors*, Chapman & Hall Ltd., London.

Muller, R., Roudier, T., Malherbe, J.M., Mein, P.: 1987, Dynamics of the solar granulation. *Publications of the Astronomical Institute of the Czechoslovak Academy of Sciences* **66**. ADS.

Muller, R., Auffret, H., Roudier, T., Vigneau, J., Simon, G.W., Frank, Z., Shine, R.A., Title, A.M.: 1992, Evolution and advection of solar mesogranulation. *Nature* **356**, 322. DOI. ADS.

November, L.J.: 1986, Measurement of geometric distortion in a turbulent atmosphere. *Appl. Opt.* **25**, 392. DOI. ADS.

November, L.J.: 1989, The vertical component of the supergranular convection. *ApJ* **344**, 494. DOI. ADS.

November, L.J.: 1994, Inferring the depth extent of the horizontal supergranular flow. *Solar Phys.* **154**, 1. DOI. ADS.

November, L.J., Simon, G.W.: 1988, Precise proper-motion measurement of solar granulation. *ApJ* **333**, 427. DOI. ADS.

November, L.J., Toomre, J., Gebbie, K.B., Simon, G.W.: 1981, The detection of mesogranulation on the sun. *ApJ* **245**, L123. DOI. ADS.

November, L.J., Simon, G.W., Tarbell, T.D., Title, A.M., Ferguson, S.H.: 1987, Large-scale horizontal flows from SOUP observations of solar granulation. In: Athay, G., Spicer, D.S. (eds.) *NASA Conference Publication* **2483**, 121. ADS.

Oda, N.: 1984, Morphological study of the solar granulation. III - The mesogranulation. *Solar Phys.* **93**, 243. DOI. ADS.

Pouquet, A., Frisch, U., Chollet, J.P.: 1983, Turbulence with a spectral gap. *Phys. Fluids* **26**, 877. DOI. ADS.

Rast, M.P., Lisle, J.P., Toomre, J.: 2004, The Spectrum of the Solar Supergranulation: Multiple Nonwave Components. *ApJ* **608**, 1156. DOI. ADS.

Requerey, I.S., Del Toro Iniesta, J.C., Bellot Rubio, L.R., Martínez Pillet, V., Solanki, S.K., Schmidt, W.: 2017, Convectively Driven Sinks and Magnetic Fields in the Quiet-Sun. *ApJS* **229**, 14. DOI. ADS.

Rieutord, M., Roudier, T., Malherbe, J.M., Rincon, F.: 2000, On mesogranulation, network formation and supergranulation. *A&A* **357**, 1063. ADS.

Rose, H.A.: 1977, Eddy diffusivity, eddy noise and subgrid-scale modelling. *J. Fluid Mech.* **81**, 719. DOI. ADS.

Roudier, T., Muller, R.: 2004, Relation between families of granules, mesogranules and photospheric network. *A&A* **419**, 757. DOI. ADS.

Roudier, T., Malherbe, J.M., November, L., Vigneau, J., Coupinot, G., Lafon, M., Muller, R.: 1997, Intergranular plumes and formation of network bright points. *A&A* **320**, 605. ADS.

Ruzmaikin, A.A., Cadavid, A.C., Chapman, G.A., Lawrence, J.K., Walton, S.R.: 1996, Spectral Properties of Solar Convection and Diffusion. *ApJ* **471**, 1022. DOI. ADS.

Scherrer, P.H., Bogart, R.S., Bush, R.I., Hoeksema, J.T., Kosovichev, A.G., Schou, J., Rosenberg, W., Springer, L., Tarbell, T.D., Title, A., Wolfson, C.J., Zayer, I., MDI Engineering Team: 1995, The Solar Oscillations Investigation - Michelson Doppler Imager. *Solar Phys.* **162**, 129. DOI. ADS.

Schwarzschild, M.: 1975, On the scale of photospheric convection in red giants and supergiants. *ApJ* **195**, 137. DOI. ADS.

Sekii, T., Kosovichev, A.G., Zhao, J., Tsuneta, S., Shibahashi, H., Berger, T.E., Ichimoto, K., Katsukawa, Y., Lites, B., Nagata, S., Shimizu, T., Shine, R.A., Suematsu, Y., Tarbell, T.D., Title, A.M.: 2007, Initial Helioseismic Observations by Hinode/SOT. *PASJ* **59**, S637. DOI. ADS.

Shine, R.A., Simon, G.W., Hurlburt, N.E.: 2000, Supergranule and Mesogranule Evolution. *Solar Phys.* **193**, 313. DOI. ADS.

Simon, G.W.: 1967, Observations of Horizontal Motions in Solar Granulation: Their Relation to Supergranulation. *Z. Astrophys.* **65**, 345. ADS.

Simon, G.W., Leighton, R.B.: 1964, Velocity Fields in the Solar Atmosphere. III. Large-Scale Motions, the Chromospheric Network, and Magnetic Fields. *ApJ* **140**, 1120. DOI. ADS.

Simon, G.W., Weiss, N.O.: 1968, Supergranules and the Hydrogen Convection Zone. *Z. Astrophys.* **69**, 435. ADS.

Simon, G.W., Weiss, N.O.: 1989, Simulation of large-scale flows at the solar surface. *ApJ* **345**, 1060. DOI. ADS.

Simon, G.W., Brandt, P.N., November, L.J., Scharmer, G.B., Shine, R.A.: 1994, Large-scale photospheric motions: first results from an extraordinary eleven-hour granulation observation. In: Rutten, R.J., Schrijver, C.J. (eds.) *NATO Advanced Science Institutes (ASI) Series C* **433**, 261. ADS.

Spruit, H.: 1997, Convection in stellar envelopes: a changing paradigm. *Mem. Soc. Astron. Ital.* **68**, 397. ADS.

Stix, M.: 2002, *The Sun, An Introduction, second edition*, Springer, Berlin.

Straus, T., Deubner, F.-L., Fleck, B.: 1992, Is mesogranulation a distinct regime of convection? *A&A* **256**, 652. ADS.

Title, A.M., Tarbell, T.D., Topka, K.P., Ferguson, S.H., Shine, R.A., SOUP Team: 1989, Statistical properties of solar granulation derived from the SOUP instrument on Spacelab 2. *ApJ* **336**, 475. DOI. ADS.

Toomre, J., Gough, D.O., Spiegel, E.A.: 1982, Time-dependent solutions of multimode convection equations. *J. Fluid Mech.* **125**, 99. DOI. ADS.

Unno, W.: 1961, On the Applicability of the Linear Theory to the Problem of Convection in Stellar Atmospheres. *PASJ* **13**, 276. ADS.

Ustyugov, S.D.: 2008, Large Eddy Simulation of Solar Photosphere Convection with Realistic Physics. In: Howe, R., Komm, R.W., Balasubramaniam, K.S., Petrie, G.J.D. (eds.) *Subsurface and Atmospheric Influences on Solar Activity*, *Astronomical Society of the Pacific Conference Series* **383**, 43. ADS.

von der Luhe, O., Dunn, R.B.: 1987, Solar granulation power spectra from speckle interferometry. *A&A* **177**, 265. ADS.

Weiss, N.O.: 1976, The Pattern of Convection in the Sun. In: Bumba, V., Kleczek, J. (eds.) *Basic Mechanisms of Solar Activity*, *IAU Symposium* **71**, 229. ADS.

Wolfram, S.: 1991, *Mathematica: a system for doing mathematics by computer, 2nd edition*, Addison-Wesley Publishing Co. Inc., Advanced Book Program, Reading, MA. ADS.

Woodard, M.F.: 2007, Probing Supergranular Flow in the Solar Interior. *ApJ* **668**, 1189. DOI. ADS.

Woodard, M.F.: 2009, Seismic Detection of Solar Mesogranular-Scale Flow. *ApJ* **706**, L62. DOI. ADS.